ARTICLE

doi:10.1038/nature11229

Deep carbon export from a Southern Ocean iron-fertilized diatom bloom

Victor Smetacek[1,2]*, Christine Klaas[1]*, Volker H. Strass[1], Philipp Assmy[1,3], Marina Montresor[4], Boris Cisewski[1,5], Nicolas Savoye[6,7], Adrian Webb[8], Francesco d'Ovidio[9], Jesús M. Arrieta[10,11], Ulrich Bathmann[1,12], Richard Bellerby[13,14], Gry Mine Berg[15], Peter Croot[16,17], Santiago Gonzalez[10], Joachim Henjes[1,18], Gerhard J. Herndl[10,19], Linn J. Hoffmann[16], Harry Leach[20], Martin Losch[1], Matthew M. Mills[15], Craig Neill[13,21], Ilka Peeken[1,22], Rüdiger Röttgers[23], Oliver Sachs[1,24], Eberhard Sauter[1], Maike M. Schmidt[25], Jill Schwarz[1,26], Anja Terbrüggen[1] & Dieter Wolf-Gladrow[1]

Fertilization of the ocean by adding iron compounds has induced diatom-dominated phytoplankton blooms accompanied by considerable carbon dioxide drawdown in the ocean surface layer. However, because the fate of bloom biomass could not be adequately resolved in these experiments, the timescales of carbon sequestration from the atmosphere are uncertain. Here we report the results of a five-week experiment carried out in the closed core of a vertically coherent, mesoscale eddy of the Antarctic Circumpolar Current, during which we tracked sinking particles from the surface to the deep-sea floor. A large diatom bloom peaked in the fourth week after fertilization. This was followed by mass mortality of several diatom species that formed rapidly sinking, mucilaginous aggregates of entangled cells and chains. Taken together, multiple lines of evidence—although each with important uncertainties—lead us to conclude that at least half the bloom biomass sank far below a depth of 1,000 metres and that a substantial portion is likely to have reached the sea floor. Thus, iron-fertilized diatom blooms may sequester carbon for timescales of centuries in ocean bottom water and for longer in the sediments.

The Southern Ocean is regarded as a likely source and sink of atmospheric CO_2 over glacial–interglacial climate cycles, but the relative importance of physical and biological mechanisms driving CO_2 exchange are under debate[1,2]. The iron hypothesis[3], which is based on iron limitation of phytoplankton growth in extensive, nutrient-rich areas of today's oceans, is that the greater supply of iron-bearing dust to these regions during the dry glacials stimulated phytoplankton blooms that, by sinking from the surface to the deep ocean, sequestered climatically relevant amounts of carbon from exchange with the atmosphere. Twelve ocean iron fertilization (OIF) experiments carried out to test this hypothesis have provided unambiguous support for the first condition: that iron addition generates phytoplankton blooms in regions with high nutrient but low chlorophyll concentrations including the Southern Ocean[4,5]. The findings are consistent with satellite observations of natural phytoplankton blooms in these regions stimulated by dust input from continental[6] and volcanic[7] sources.

The timescales on which CO_2 taken up by phytoplankton is sequestered from the atmosphere depend on the depths at which organic matter sinking out of the surface layer is subsequently remineralized back to CO_2 by microbes and zooplankton. In the Southern Ocean, the portion of CO_2 retained within the 200-m-deep winter mixed layer would be in contact with the atmosphere within months, but carbon sinking to successively deeper layers, and finally the sediments, will be sequestered for decades to centuries or longer. Previous OIF experiments have not adequately demonstrated the fate and depth of sinking of bloom biomass[5], so it is uncertain whether mass, deep-sinking events comparable to those observed in the aftermath of natural blooms[8] also ensue from OIF blooms. Furthermore, palaeo-oceanographic proxies from the underlying sediments are ambiguous regarding productivity of the glacial Southern Ocean[1,2,9,10]. Hence, the second condition of the iron hypothesis, that OIF-generated biomass sinks to greater depths, has yet to be confirmed. The issue is currently receiving broad attention because OIF is one of the techniques listed in the geoengineering portfolio to mitigate the effects of climate change[11].

Monitoring the sinking flux from an experimental bloom requires vertical coherence between surface and deeper layers, a condition fulfilled by the closed cores of mesoscale eddies formed by meandering frontal jets of the Antarctic Circumpolar Current, which are prominent in satellite altimeter images as sea surface height anomalies[12]. An

[1]Alfred Wegener Institute for Polar and Marine Research, Am Handelshafen 12, 27570 Bremerhaven, Germany. [2]National Institute of Oceanography, Dona Paula, Goa 403 004, India. [3]Norwegian Polar Institute, Fram Centre, Hjalmar Johansens Gate 14, 9296 Tromsø, Norway. [4]Ecology and Evolution of Plankton, Stazione Zoologica Anton Dohrn, Villa Comunale, 80121-Napoli, Italy. [5]Johann Heinrich von Thünen Institute, Institute of Sea Fisheries, Palmaille 9, 22767 Hamburg, Germany. [6]Department of Analytical and Environmental Chemistry, Vrije Universiteit Brussel, Pleinlaan 2, 1050 Brussels, Belgium. [7]Univ. Bordeaux/CNRS, EPOC, UMR 5805, Station Marine d'Arcachon, 2 rue du Professeur Jolyet, F-33120 Arcachon, France. [8]Oceanography Department, University of Cape Town, Private Bag X3, Rondebosch, 7701 Cape Town, South Africa. [9]LOCEAN-IPSL, CNRS/UPMC/IRD/MNHN, 4 Place Jussieu, 75252 Paris Cedex 5, France. [10]Department of Biological Oceanography, Royal Netherlands Institute for Sea Research, PO Box 59, 1790 AB Den Burg, The Netherlands. [11]Department of Global Change Research, Instituto Mediterraneo de Estudios Avanzados, CSIC-UIB, Miquel Marques 21, 07190 Esporles, Mallorca, Spain. [12]Leibniz Institute for Baltic Sea Research Warnemünde, Seestraße 15, 18119 Rostock, Germany. [13]Bjerknes Centre for Climate Research, University of Bergen, Allegaten 55, N-5007 Bergen, Norway. [14]Norwegian Institute for Water Research, Thormøhlensgate 53 D, 5006 Bergen, Norway. [15]Department of Environmental Earth System Science, Stanford University, Stanford, California 94305, USA. [16]Helmholtz Centre for Ocean Research Kiel, Düsternbrooker Weg 20, 24105 Kiel, Germany. [17]Earth and Ocean Sciences, School of Natural Sciences, National University of Ireland, Galway, Quadrangle Building, University Road, Galway, Ireland. [18]Phytolutions GmbH, Campus Ring 1, 28759 Bremen, Germany. [19]Department of Marine Biology, University of Vienna, Althanstrasse 14, 1090 Vienna, Austria. [20]School of Environmental Sciences, University of Liverpool, Room 209 Nicholson Building, 4 Brownlow Street, Liverpool L69 3GP, UK. [21]Wealth from Oceans Flagship, Commonwealth Scientific and Industrial Research Organisation, Castray Esplanade, Hobart, Tasmania 7000, Australia. [22]MARUM – Center for Marine Environmental Sciences, University of Bremen, Leobener Strasse, D-28359 Bremen, Germany. [23]Institute for Coastal Research, Helmholtz-Zentrum Geesthacht, Center for Materials and Coastal Research, Max-Planck-Strasse 1, 21502 Geesthacht, Germany. [24]Eberhard & Partner AG, General Guisan Strasse 2, 5000 Arau, Switzerland. [25]Centre for Biomolecular Interactions Bremen, FB 2, University of Bremen, Postfach 33 04 40, 28359 Bremen, Germany. [26]School of Marine Science & Engineering, Plymouth University, Drake Circus, Plymouth PL4 8AA, UK.
*These authors contributed equally to this work.

added advantage offered by closed eddy cores is that processes occurring in the fertilized patch can be compared with natural processes in adjoining unfertilized waters of the same provenance.

The eddy and experiment

The European Iron Fertilization Experiment (EIFEX) was carried out from 11 February 2004 to 20 March 2004 during RV *Polarstern* cruise ANT XXI/3, in the clockwise-rotating core of an eddy formed by a meander of the Antarctic polar front (Fig. 1 and Supplementary Information). The eddy was mapped over a period of seven days shortly after fertilization of the patch with a grid of 80 stations along eight north–south transects 9 km apart. The rotating patch was encountered on two of the grid transects. Measurements of current speed and direction with the vessel-mounted acoustic Doppler current profiler and images of sea surface height anomalies revealed a closed, 60-km-diameter core clearly demarcated from the surrounding meander of the Antarctic polar front in all measured physical, chemical and biological properties (Fig. 1a, b and Supplementary Information).

Estimates of geostrophic shear and transports derived from temperature and salinity profiles (Supplementary Figs 1 and 2) indicate a coherent surface-to-bottom eddy circulation that was almost closed

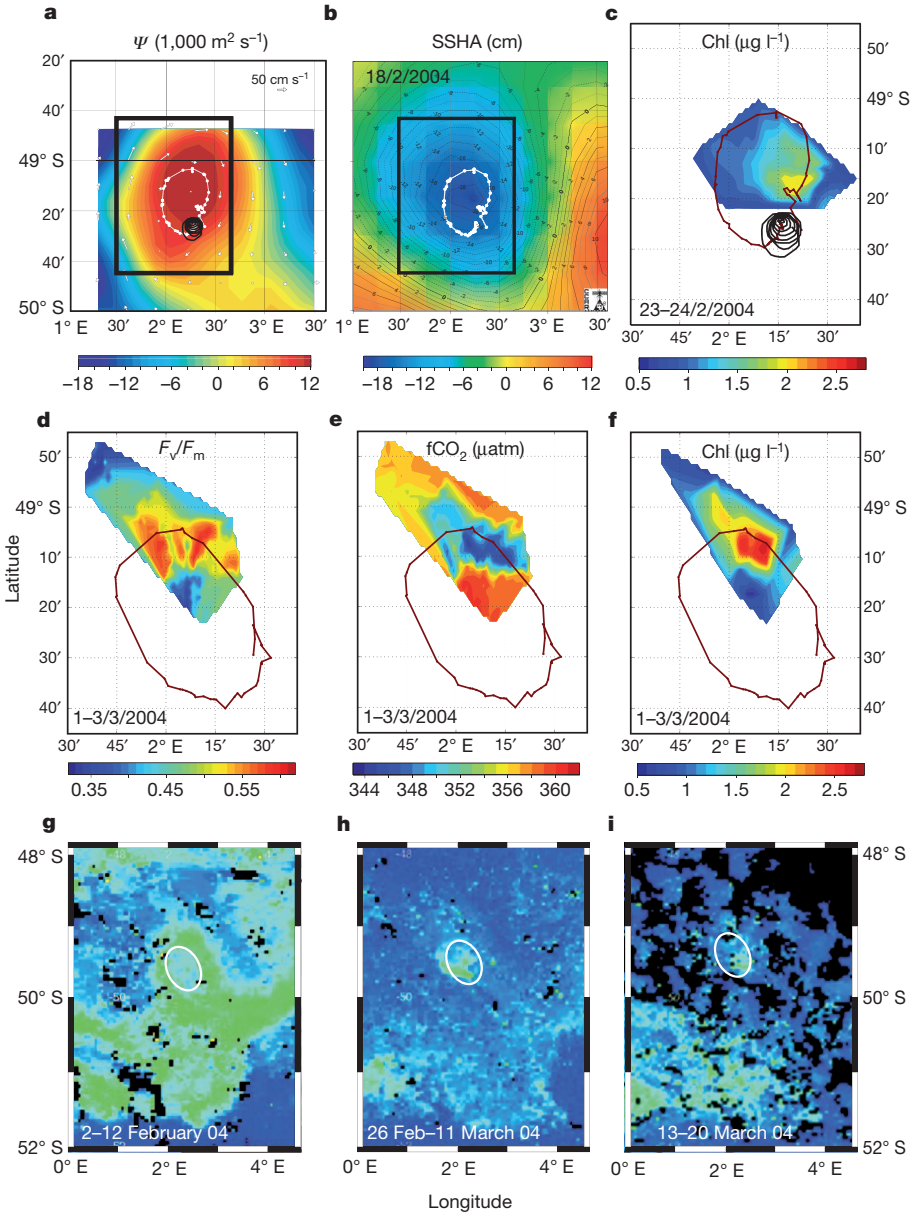

Figure 1 | Experimental eddy and the fertilized patch. **a**, The eddy core depicted with the stream function (Ψ; contours and colour scale) derived from currents measured using a vessel-mounted acoustic Doppler current profiler at a regular grid of stations between days 1 and 7. The black spiral is the ship's track (a Lagrangian circle) around the buoy drifting southwestward during fertilization. The white line is the superimposed track of the drifting buoy during its first rotation from days −1 to 11 (same as in **b** and **c**). **b**, Altimeter image of sea surface height anomaly (SSHA; contours and colour scale from CCAR, http://argo.colorado.edu/~realtime/gsfc_global-real-time_ssh/.) The rectangle in **a** and **b** is enlarged in **c**–**f**. **c**, Area and location of the patch on days 10 and 11 after fertilization, depicted on the basis of chlorophyll measurements. The yellow area is the hot spot. **d**–**f**, Location and area of the patch 17 days after fertilization, depicted in terms of photochemical efficiency (F_v/F_m; **d**), CO_2 fugacity (fCO_2; **e**) and chlorophyll concentration (**f**). The line is the track of the drifting buoy during its second rotation (days 13–21). The red area in **f** is the hot spot. **g**–**i**, Satellite-derived surface chlorophyll concentrations of the EIFEX eddy before fertilization (**g**), during the bloom peak (**h**) and in its demise phase (**i**). The eddy core is encircled in white; the EIFEX bloom is evident in **h** and **i** (green colour is >1 μg Chl l^{-1}). Note the natural bloom along the Antarctic polar front, which disappeared in this period. SeaWiFS images (**g**–**i**) courtesy of the NASA SeaWiFS Project and GeoEye.

and had little divergence. The vertical coherence of the eddy was also revealed by the congruent tracks of four neutrally buoyant floats positioned at respective depths of 200, 300, 500 and 1,000 m (Supplementary Fig. 3). A post-cruise Lagrangian analysis based on delayed-time altimetry[13] showed that, for the entire duration of the experiment, the compact core was only marginally eroded by lateral stirring, losing less than 10% of its content in total (Supplementary Information). This finding is consistent with diffusive heat budgets derived from the observed warming of the eddy's cold core[14]. Hence, the EIFEX eddy provided ideal conditions for monitoring the same water column from the surface to the sea floor over time.

The site of the pre-fertilization control station was marked with a drifting buoy around which a circular patch of 167 km^2 was fertilized with dissolved Fe(II) sulphate on 12–13 February (day 0) to yield a concentration of 1.5 μmol Fe m^{-3} in the 100-m-deep surface mixed layer, which is greater than background values by a factor of around five. A second fertilization on days 13 and 14 added an additional 0.34 μmol Fe m^{-3} to the 100-m-deep surface layer of the spreading patch. The patch was inadvertently placed off-centre but well within the closed eddy core and completed four rotations during the experiment. The area of the patch increased from 167 km^2 on day 0 to 447 km^2 on day 11 and to 798 km^2 on day 19 (Fig. 1c–f and Supplementary Information). 'In-stations' were taken in the least-diluted region of the patch: the 'hot spot' (Fig. 1c–f). 'Out-stations' were taken within the eddy core well away from the patch but in different locations relative to it, and hence did not represent ideal controls for quantifying processes within the patch.

Sampling frequency and depth coverage by discrete measurements are illustrated by the vertical distributions of chlorophyll and silicate concentrations (Fig. 2). Vertical profiles from *in situ* recording instruments indicated that the boundary of the mixed layer, defined by a sharp dip in temperature, salinity, fluorescence and transmission, was generally at a depth of 100 m (ref. 15; 97.6 ± 20.6 m). The element and biomass budgets presented here are based on inventories (in moles or grams per square metre) derived from the trapezoidal integration of six to eight discrete measurements from the 100-m-deep surface layer. For comparison with other studies, the stocks (inventories) from this layer are also presented where appropriate as depth-averaged concentrations (in millimoles or milligrams per cubic metre).

Processes inside and outside the patch

Enhanced phytoplankton growth stimulated by iron fertilization resulted in highly significant, linear increases in stocks of chlorophyll (Chl), particulate organic carbon (POC), nitrogen (PON), phosphate (POP) and biogenic silica (BSi) until day 24 (Figs 2a and 3). These stocks, depicted as depth-averaged concentrations in Fig. 3, declined thereafter, although at different rates. However, inventories of the corresponding dissolved nutrients, including dissolved organic nitrogen (DON), underwent a constant, linear decline until the end of the experiment, indicating that the respective uptake rates were maintained throughout (Fig. 3). Detailed, visual, quantitative examination of organisms and their remains across the entire size spectrum of the plankton revealed that population growth of many different species of large diatoms accounted for 97% of the Chl increase. The decline after day 24 was caused by mass death and formation of rapidly sinking aggregates by some diatom species, which was partly compensated by continued growth of other, heavily silicified species with high accumulation rates. The strikingly linear, instead of exponential, trends can be attributed to the effects of patch dilution with surrounding water because dilution rates (0.06–0.1 d^{-1}; Supplementary Information) and phytoplankton accumulation rates (0.03–0.11 d^{-1}) were similar.

The discrepancies in the budgets of particulate and dissolved pools of the various elements in the surface layer can only be explained by the sinking out of particles, as losses to dissolved organic pools can largely be ruled out: stocks of dissolved organic carbon (DOC) remained stable (44 ± 2 mmol C m^{-3}; Fig. 3l), those of DON halved (from 3.8 to 2.0 mmol N m^{-3}; Fig. 3f) and those of dissolved organic phosphate (not shown) were at the detection limit. The decline in DON was barely reflected in DOC because it was apparently associated with a relatively small, labile fraction with much lower C/N ratios than that of the large refractory DOC pool.

The post-fertilization eddy survey revealed that the patch was located in the region of the eddy core with the highest silicate and lowest chlorophyll concentrations (~0.7 mg Chl m^{-3}; Supplementary Information). Patchy, natural blooms, probably caused by local dust input along the Antarctic polar front[6], had occurred before our arrival adjacent to the patch (Fig. 1g), as indicated by lower nutrient and higher Chl stocks (up to 1.2 mg Chl m^{-3}) and higher particle loads in subsurface layers (Supplementary Information). These

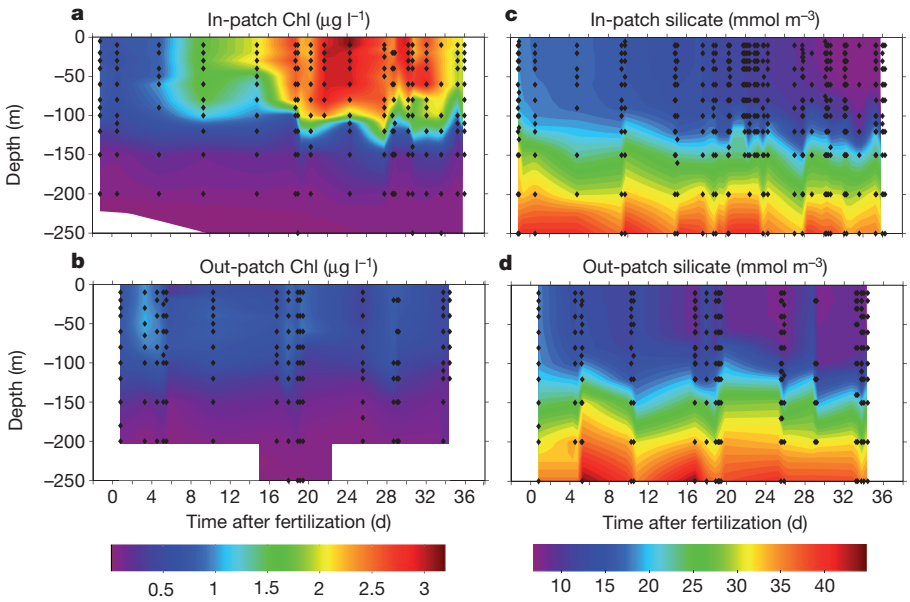

Figure 2 | Temporal evolution of chlorophyll and silicate concentrations. **a**, Chlorophyll concentrations reflect the growth, peak and demise phases of the bloom in the patch. **b**, By comparison, the Chl concentration outside the patch is low. The slightly higher out-patch values soon after fertilization are due to local patchiness in outside water and not to interim accumulation. **c**, **d**, The declining trend of silicate in outside water (**d**) is interrupted by local patchiness, whereas within the patch the trend is smooth (**c**). Note the variations in mixed-layer depth below 100 m. Black diamonds indicate depths of discrete samples.

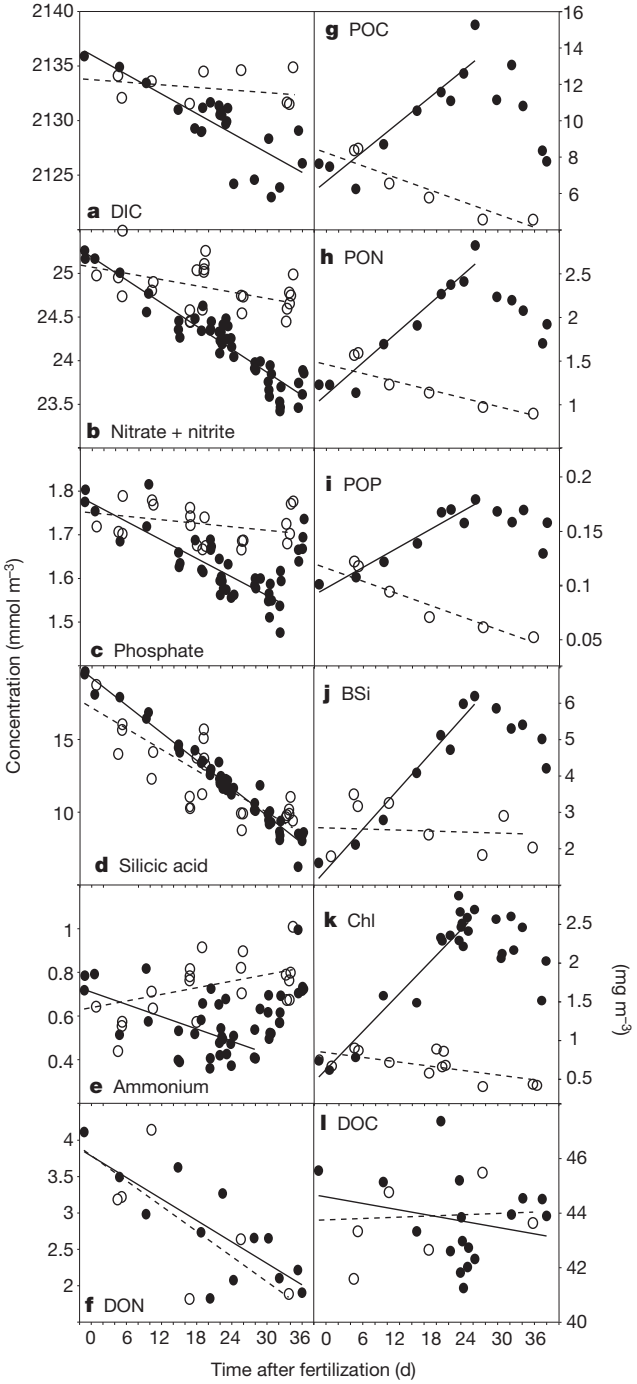

Figure 3 | Temporal evolution of dissolved and particulate elements. Values inside (filled circles) and outside (open circles) the fertilized patch are depth-integrated average concentrations for the upper 100 m of the water column. All concentrations are in millimoles per cubic metre except that for Chl (**k**), which is expressed in milligrams per cubic metre. Lines represent the temporal evolution inside (solid line) and outside (broken line) the fertilized patch used in elemental budget calculations (Supplementary Methods) determined by linear regression. Inside the patch, the r^2 values for the models are 0.64 (DIC; **a**), 0.88 (nitrate plus nitrite; **b**), 0.74 (phosphate; **c**), 0.97 (silicic acid; **d**), 0.33 (ammonium; **e**), 0.63 (DON; **f**), 0.84 (POC; **g**), 0.94 (PON; **h**), 0.93 (POP; **i**), 0.96 (BSi; **j**), 0.92 (Chl; **k**) and 0.05 (DOC; **l**). Outside the patch, the r^2 values are 0.06 (DIC), 0.24 (nitrate plus nitrite), 0.13 (phosphate), 0.71 (silicic acid), 0.24 (ammonium), 0.58 (DON), 0.84 (POC), 0.64 (PON), 0.85 (POP), 0.008 (BSi) and 0.005 (DOC). All regressions are significant ($P < 0.005$) with the exception of in-patch DOC ($P = 0.4$) and out-patch DIC ($P = 0.5$), nitrate plus nitrite ($P = 0.011$), phosphate ($P = 0.1$), ammonium ($P = 0.02$), DON ($P = 0.046$), PON ($P = 0.03$), BSi ($P = 0.8$) and DOC ($P = 0.8$).

natural blooms sank from the surface in the first week, as corroborated by barite profiles in subsurface layers[16], and, hence, greater particle stocks encountered at depth at some out-stations probably stemmed from them. Particle stocks (except those of BSi) in the upper 100-m-deep layer outside the patch continued declining by about 50% during the five weeks of the experiment (Fig. 3) as a result of steady sinking out of particles, as indicated by the discrepancy between the temporal evolutions of dissolved and particulate inventories of the respective elements. On a visit to the eddy core on day 50, we found that Chl concentrations had declined further, to 0.1 mg Chl m^{-3}.

Export from the iron-induced bloom

Vertical particle flux (export) induced by iron fertilization was estimated for the hot spot from losses of biogenic element inventories in the surface layer, including ^{234}Th; the increase in POC in the underlying deep water column; and by balancing rates of primary production and heterotrophic activity. These estimates represent the total export and include losses incurred by the surface layer in the absence of fertilization (background flux). Because some out-stations were affected by patchy natural blooms within the eddy core, they did not represent ideal controls. However, export rates from the fertilized patch, estimated from elemental budgets in the surface layer (0–100 m) and particularly POC increments between depths of 200 and 500 m until day 24, were remarkably similar to the corresponding values from outside water (Fig. 4), indicating little additional flux from the growing bloom. Export from the patch increased steeply after day 24, but outside loss rates remained constant. Hence, we assume that the background flux from the patch also remained constant until the end of the experiment but was overridden by the iron-induced flux event starting between days 24 and 28. We estimate the total background export from the patch by extrapolating the flux between days 0 and 24 to day 36, and subtract this amount from the total export to obtain the iron-induced export (Supplementary Methods).

Element losses

A conservative estimate for the export of biogenic elements from the 100-m-deep surface layer in the hot spot is the difference between the decline in dissolved inventories (nutrient uptake) and concomitant accumulation in particulate stocks (Supplementary Table 1). Uptake was calculated from the linear regressions depicted in Fig. 3a–f. Accumulation was estimated as the difference between final and initial stocks of BSi, POP, PON and POC. Initial stocks of particulate elements were taken from the intercept on day 0 of the linear regressions until day 24, and final stocks were the values measured on day 36 (Fig. 3g–j). The decline in the inventory of dissolved inorganic carbon (DIC), of 1.1 mol m^{-2}, underestimates the actual uptake by phytoplankton because of atmospheric CO_2 replenishment. Correcting for air–sea gas exchange adds 0.4 mol m^{-2} to the uptake and, hence, also to export. The background flux was obtained by extrapolating the losses estimated until day 24 (0.3 mol C m^{-2}) to the values on day 36. The iron-induced export, of 0.9 mol C m^{-2} (79 mmol C m^{-2} d^{-1} for the 12-day flux event), was obtained by subtracting the background flux from the total flux estimates (1.4 mol C m^{-2}) for the 36 days of the calculations (Supplementary Table 1).

Correcting budgets with the measured values presented above for mixed-layer deepening and diapycnal mixing using the diffusion coefficient of 3.3×10^{-4} m^2 s^{-1} estimated for the EIFEX eddy core[14] almost doubles the estimates of background export inside the hot spot (from 0.4 to 0.9 mol C m^{-2}, or 12 to 26 mmol C m^{-2} d^{-1}) and outside the fertilized patch (from 0.7 to 1.2 mol C m^{-2}, or 21 to 36 mmol C m^{-2} d^{-1}). Because nutrient input to the surface layer from below was relatively constant during the experiment, the correction for iron-induced export during the last 12 days was comparatively minor: from 0.9 to 1.1 mol C m^{-2}, or 79 to 98 mmol C m^{-2} d^{-1}. Furthermore, correcting the hot-spot budgets for the effects of

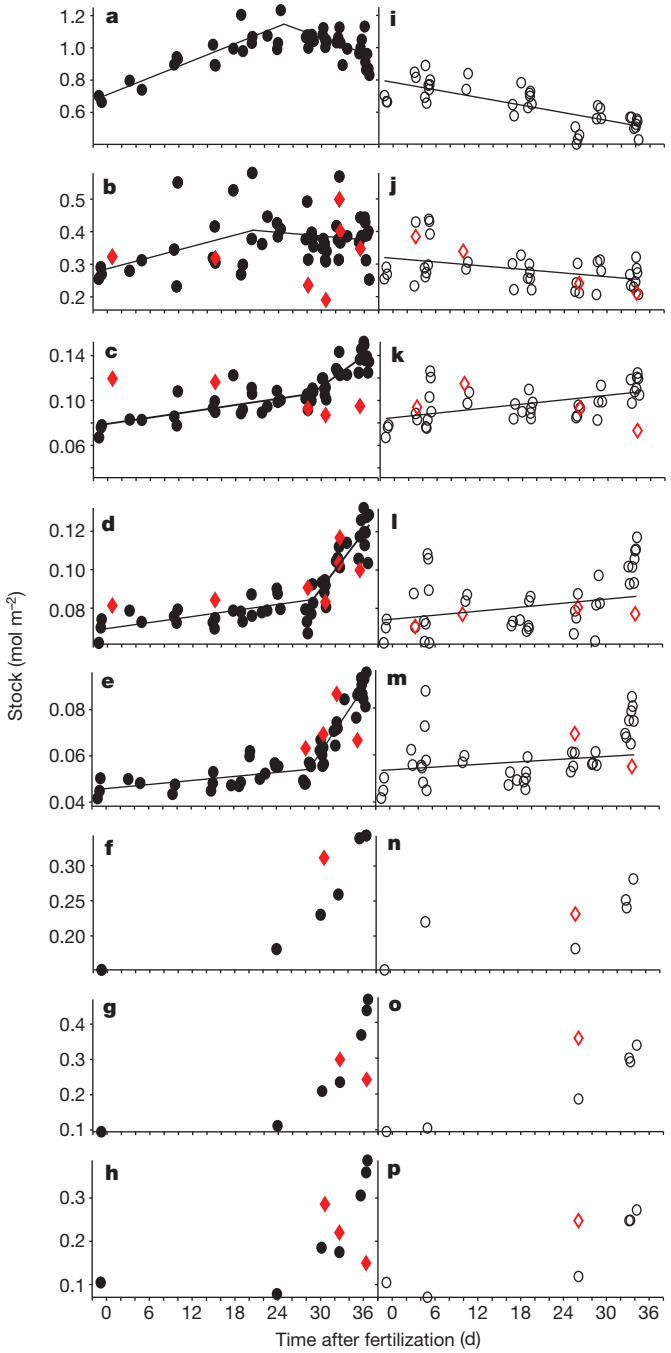

Figure 4 | Temporal evolution of particulate organic carbon stocks in successive depth layers. Stocks for the respective layers are derived from depth-integrated, vertical profiles of beam attenuation of a transmissometer calibrated using discrete POC measurements (black symbols). Filled and open symbols show data inside and outside the patch, respectively. Depth intervals of integrations are 0–100 m (**a**, **i**), 100–200 m (**b**, **j**), 200–300 m (**c**, **k**), 300–400 m (**d**, **l**), 400–500 m (**e**, **m**), 500–1,000 m (**f**, **n**), 1,000–2,000 m (**g**, **o**) and 2,000–3,000 m (**h**, **p**). Lines are derived from linear regression models. Variability in stocks and trends in the layers at 100–200 m (**b**, **j**) is due to intermittent shoaling and deepening of the particle-rich, surface mixed layer between 100 and 120 m, possibly as a result of the passage of internal waves. The high out-patch values on days 5 and 34 are not included in the regressions. The layer below 3,000 m is not included to avoid contamination by resuspended sediments in the nepheloid layer. Red diamonds show integrated stocks from measurements on discrete water samples. Variability in these values is due to low depth resolution, particularly below 500 m.

horizontal dilution (patch spreading) increases the total DIC uptake to 2.4 mol C m^{-2}, of which 0.6 mol C m^{-2} is exported laterally (Table 1). However, the increase of iron-induced export to 1.2 mol m^{-2} is again minor (Table 1). Dividing the total DIC uptake (2.4 mol C m^{-2}) by the total amount of iron added to the patch water column (0.18 mmol Fe m^{-2}) yields a C/Fe ratio of 13,000 ± 1,000 (s.e.m.). This ratio is conservative for reasons discussed in Supplementary Information.

Nitrate (nitrate plus nitrite) uptake until the bloom peak on day 24 (0.17 mol m^{-2}) accounted for 80% of PON production (0.21 mol N m^{-2}), resulting in negative values for background flux not indicated by the other elements (Supplementary Table 2). The decline in DON, through uptake by bacteria and excretion as ammonium to phytoplankton, more than compensates for the N deficit, but its origin is enigmatic. The same amount of DON, but much less DIC, nitrate and phosphate, were taken up outside the patch (Fig. 3 and Supplementary Table 3); hence DON contribution to export outside the patch is likely to have been similar to that inside the patch. The high variability in ammonium stocks (Fig. 3e) is consistent with rapid turnover within this pool. No clear trends were observed in the subsurface ammonium maxima inside and outside the patch (Supplementary Fig. 4), indicating minor additional accumulation of breakdown products from the flux event in the subsurface layer. The C/N ratio for iron-induced export (8.5) is higher than the POC/PON ratio of suspended elements (~5), a result that was also observed during the Southern Ocean Iron Experiment[4].

The steep increase in phosphate stocks on days 35 and 36 (Fig. 3c) is only partly explained by leaching from autolysed cytoplasm, owing to the well-established greater mobility of this element relative to carbon[17]. Hence, the negative value for exported P due to fertilization (Table 1) is difficult to explain, because unlike for N, the source of the additional phosphate during the last two days is unknown. Approximately 65% of the silicate taken up was exported during the 36 days, of which half can be attributed to iron-induced export at a C/Si ratio of 3 and the other half to background flux at a C/Si ratio of 0.8. Outside the patch, silicate uptake was slightly lower than inside but all of it was exported in the same period at a C/Si ratio of 0.9, which we attribute to the activity of diatom species that selectively sink silica.

POC export rates from the hot spot estimated from ^{234}Th increased steeply from background values <40 mmol C m^{-2} d^{-1} to 125 mmol C m^{-2} d^{-1} during days 28–32, but declined thereafter presumably owing to uncertainties associated with short-term sampling by this method (Supplementary Information). Nevertheless, the two peak values during the flux event are the highest recorded so far in the Southern Ocean.

Transmissometer profiles

Beam attenuation of the profiling transmissometer was highly correlated with discrete POC measurements across the entire range of concentrations encountered ($r^2 = 0.934$ and $P < 0.001$, where r is the correlation coefficient and P is the observed significance level; Supplementary Fig. 5). Because of the high-resolution vertical coverage of the water column, the depth-integrated transmissometer profiles provide a record of POC accumulation and depletion over depth and time from which export can be estimated[18].

Integrated POC stocks in the upper 3,000 m of the water column of the patch increased over 36 days by 1.3 ± 0.2 mol C m^{-2} (s.d.; Fig. 5), implying an accumulation rate of 38 mmol C m^{-2} d^{-1}. The flux event after day 24 is signalled by steeply increasing POC stocks in the water column below 200 m (Fig. 4). These stocks reached 0.8 ± 0.1 mol C m^{-2} (s.d.) above background levels on day 36, of which 0.7 ± 0.1 mol C m^{-2} (s.d.) was below 500 m (Fig. 5). The increase in deep POC stocks is reasonably close to the corrected estimate of iron-induced export from the surface layer budget (1.2 ± 0.4 mol C m^{-2} (s.d.)), given that some POC had already reached the deep-sea floor, as indicated by fresh diatom cells and labile pigments found close to the bottom (Supplementary Fig. 7). Hence, losses of iron-induced sinking flux due to ongoing respiration were apparently minor. Profiles of biogenic

Table 1 | Total and iron-induced export from the hot spot of the fertilized patch

	Days	Si	P	$NO_2 + NO_3$	Total N	C
Decrease in stocks of dissolved elements	0–36	1.14 ± 0.03	0.007 ± 0.003	0.160 ± 0.008	0.33 ± 0.08	1.1 ± 0.2
Input due to air–sea gas exchange	0–36	—	—	—	—	0.4
Dissolved-element input from vertical mixing (diapycnal mixing and deepening of the mixing layer)	0–36	0.22 ± 0.01	0.011 ± 0.0008	0.059 ± 0.004	0.10 ± 0.01	0.6 ± 0.2
Dissolved-element input from horizontal mixing (dilution effect)	0–36	~0	0.010 ± 0.001	0.061 ± 0.005	0.08 ± 0.03	0.27 ± 0.06
Total uptake (decrease in dissolved stocks plus gas exchange plus vertical mixing plus horizontal mixing)	0–36	1.36 ± 0.03	0.028 ± 0.003	0.28 ± 0.01	0.50 ± 0.09	2.4 ± 0.2
Difference between final and initial particulate-matter standing stocks	0–36	0.28 ± 0.02	0.0062 ± 0.0005	0.081 ± 0.009	0.081 ± 0.009	0.11 ± 0.07
Particulate matter loss by horizontal mixing (dilution effect)	0–36	0.19 ± 0.02	0.0089 ± 0.0004	0.110 ± 0.006	0.110 ± 0.006	0.58 ± 0.04
Vertical export (total uptake minus difference in particulate stocks minus particulate loss by horizontal mixing)	0–36	0.89 ± 0.04	0.013 ± 0.003	0.09 ± 0.02	0.31 ± 0.09	1.7 ± 0.2
Background (vertical) export*	0–36	0.50 ± 0.07	0.025 ± 0.003	−0.06 ± 0.03	0.18 ± 0.06	0.5 ± 0.3
Vertical export due to fertilization (vertical export minus background export)	24–36	0.40 ± 0.08	−0.012 ± 0.005	ND	0.1 ± 0.1	1.2 ± 0.4

Budgets were calculated for the surface layer (0–100 m) starting immediately after fertilization (day 0) and lasting until the last station where nutrients were measured inside the fertilized patch (day 36) (see Supplementary Methods for details). Total N includes $NO_2 + NO_3$, DON and ammonium. All values are in moles per square metre. Uncertainties (s.e.m.) were estimated by propagation of standard errors based on linear uptake models (Fig. 3) and measurement uncertainties. ND, not determined.
* Vertical export between days 0 and 24 (0.4 mol C m^{-2}; Supplementary Table 3) extrapolated to days 0–36 (Supplementary Methods).

barite[16] indicate that only ~11% of POC exported during the flux event was remineralized between depths of 200 and 1,000 m. By contrast, the background export until day 24 was largely respired above 500 m, because the POC increase below 200 m (Fig. 4) amounted to 0.04 mol C m^{-2}, which is <10% of the concomitant loss from the surface layer calculated from corrected element budgets. Identical rates of POC increase in subsurface layers outside the patch also indicate that background export was remineralized above 500 m.

We attribute the comparatively high POC stocks in outside waters (0.5 ± 0.1 mol C m^{-2} (s.d.) above background) between 200 and 1,000 m on day 5 and between 300 and 3,000 m on days 33 and 34 (Fig. 4) to slower sinking particle flux from the patchy natural blooms mentioned above (Supplementary Information). Local patchiness in out-stations is indicated by greater scatter in values from successive profiles taken during the same station than in in-stations (Figs 4 and 5).

The steep increase in POC stocks below 200 m under the patch after day 28 (Fig. 4) can be attributed to POC in the mucilaginous matrix of diatom aggregates in the >1-mm size range, which appeared as spikes in the transmissometer profiles. The occurrence of large aggregates reflected in spikiness of the profiles was notably higher under the hot spot than outside it (Supplementary Fig. 6). Sinking rates of >500 m d^{-1} and aggregates in the centimetre size range are required to account for the similar slopes of increasing POC at all depths down to the sea floor after day 28, just four days after the enhanced appearance of spikes (aggregate formation) at the pycnocline (Supplementary Fig. 6a) and visual observation of mass mortality in a major, spiny diatom species, *Chaetoceros dichaeta*. By contrast, the smaller aggregates from the less dense natural blooms sank more slowly than those from the patch. Coagulation models[19,20] of aggregate formation confirm the relationships between sinking rate and bloom density and, respectively, cell size (including spine length). The latter depends on the species composition of the bloom, which thus has a decisive role in the long-term fate of its biomass.

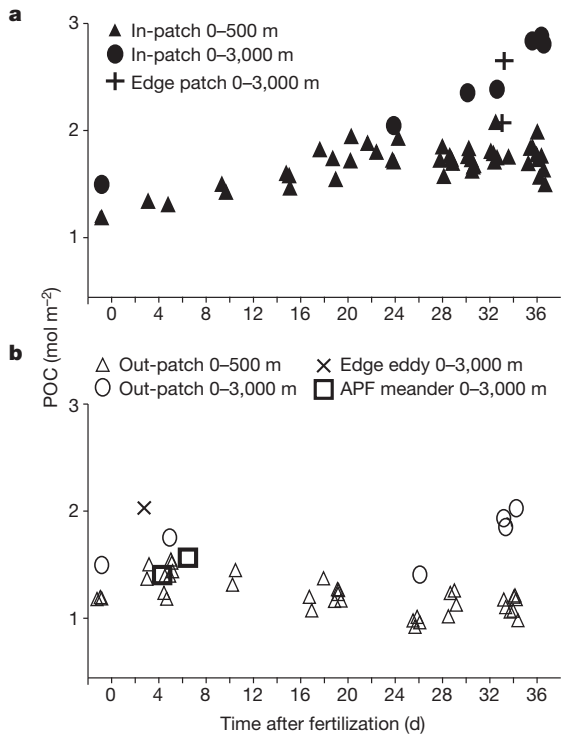

Figure 5 | Depth-integrated particulate organic carbon stocks. Stocks for the 0–500-m (triangles) and 0–3,000-m (circles) water columns are derived from vertical transmissometer profiles as in Fig. 4. Filled and open symbols show data inside and outside the patch, respectively. All profiles measured down to the sea floor during the study are depicted. Because the depth of the flux event was not anticipated and deep casts are time consuming, only six profiles to the sea floor were measured before the flux event: one before fertilization, one in the hot spot, two outside the patch (of which one was inside the core) and two in the meander of the Antarctic polar front (APF).

Organism stocks and rates

Biomass estimates from organism counts were highly correlated with the respective bulk measurements: the ratio of POC to phytoplankton carbon was 1.4 mol mol^{-1} ($r^2 = 0.54$, $P < 0.0001$), that of phytoplankton carbon to Chl was 27 mg mg^{-1} ($r^2 = 0.87$, $P < 0.0001$) and that of BSi to total diatom carbon was 0.9 mol mol^{-1} ($r^2 = 0.76$, $P < 0.0001$). This indicated that accumulation of particulate organic detritus was minor, that POC increments had a high cellular chlorophyll content as a result of newly accumulated biomass (POC/Chl = 32 mg mg^{-1}, $r^2 = 0.394$, $P < 0.0001$) and that new biomass was dominated by diatoms. Rates of primary production doubled following fertilization and stabilized at 0.13 mol C m^{-2} d^{-1} (1.5 ± 0.1 g C m^{-2} d^{-1}) from days 9 to 35 but declined to 0.08 mol C m^{-2} d^{-1} on day 36. The total C accumulation and export rates estimated from element budgets are easily accommodated in the organic carbon produced during the bloom (4.2 mol C m^{-2}, or 51 g C m^{-2}). The remainder could be attributed to recycling in the surface layer by bacteria, microzooplankton and copepods, whereby grazing pressure on the diatoms was lower than on other protists. Bacterial stocks and production rates declined by ~30% in the demise phase of the bloom, which supports the high transfer efficiency of POC to depth. Thus, the budgets of biological rates are remarkably consistent with other budgets.

In outside water, primary production amounted to 1.36 mol C m^{-2} (16 g C m^{-2}) over 34 days, which is too low to accommodate the estimated sinking losses of 1.2 mol C m^{-2} (14.4 g C m^{-2}; Supplementary Table 3) because bacterial remineralization rates and copepod grazing pressure were in the same range outside the patch as inside. The

discrepancy between measured production and estimated loss rates is partly due to three out-stations placed where there had been previous natural blooms with comparatively low surface DIC inventories (Fig. 3a) but where much of the corresponding POC stocks had already sunk to subsurface layers. Furthermore, the vertical diffusion coefficient applied[14] seems to lead to an overestimation of export. Applying another, twofold-higher, diffusion coefficient for diapycnal mixing derived from microstructure profiles during EIFEX[15] results in twofold-higher export values that are supported even less by direct observations of the plankton community and by POC profiles.

Conclusions

The peak chlorophyll stock of 286 mg m^{-2} is the highest recorded in an OIF experiment so far[5] and demonstrates that, contrary to the current view[21], a massive bloom can develop in a mixed layer as deep as 100 m. The EIFEX results provide support for the second condition of the iron hypothesis[4], that mass sinking of aggregated cells and chains in the demise phase of diatom blooms also occurs in the open Southern Ocean, both in natural[22,23] and in artificially fertilized blooms. Given the large sizes, high sinking rates and low respiratory losses of aggregates from the iron-induced bloom, much of the biomass is likely to have been deposited on the sea floor as a fluff layer[24] with carbon sequestration times of many centuries and longer. Larger-scale, longer-term OIF experiments will be required to reduce the effects of horizontal dilution and to explore further the potential of this technique for hypothesis testing in the fields of ecology, biogeochemistry and climate.

METHODS SUMMARY

The eddy was selected on the basis of satellite altimetry and surface chlorophyll distribution. Fertilization was carried out by releasing 7 t of commercial Fe(II) sulphate dissolved in 54 m^3 of acidified (HCl) sea water into the ship's propeller wash while spiralling out from a drifting buoy at 0.9-km radial intervals. By day 14, the initial 167-km^2 patch had spread and an area of 740 km^2 was again fertilized with 7 t of Fe(II) sulphate, this time along east–west transects 3 km apart, from north to south in the direction of the moving patch (Fig. 1c).

The patch was located using the drifting buoy, and the photochemical efficiency (F_v/F_m) was measured continuously with a fast-repetition-rate fluorometer. As in previous experiments, F_v/F_m was significantly higher in iron-fertilized water. Within a week, the bloom had accumulated sufficient biomass that additional tracers (chlorophyll concentration and continuous measurements of fCO_2) could be used to locate the part of the patch least affected by dilution with outside water, that is, that with the highest chlorophyll concentration and, in the last week, the lowest fCO_2 value (Fig. 1c–f). All in-stations were placed inside this hot spot and care was taken to locate it with small-scale surveys before sampling and to keep the ship within it during sampling at each station, which generally lasted about 8 h. Some in-stations were within the patch but were subsequently shown to have missed the hot spot and have therefore been excluded. For logistical reasons, the out-stations were taken in different locations of the core relative to the direction of the moving patch, that is, ahead, behind or diagonally opposite it.

Standard oceanographic methods and instruments[15] were used to collect samples and measure the properties of the water column. See Supplementary Information for details.

Received 15 November 2011; accepted 3 May 2012.

1. Sigman, D. M. Hain, M. P. & Haug, G. H. The polar ocean and glacial cycles in atmospheric CO_2 concentration. *Nature* **466,** 47–55 (2010).
2. Anderson, R. F. *et al.* Wind-driven upwelling in the Southern Ocean and the deglacial rise in atmospheric CO_2. *Science* **323,** 1443–1448 (2009).
3. Martin, J. H. Glacial-interglacial CO_2 changes: the iron hypothesis. *Paleoceanography* **5,** 1–13 (1990).
4. Coale, K. H. *et al.* Southern Ocean iron enrichment experiment: carbon cycling in high- and low-Si waters. *Science* **304,** 408–414 (2004).
5. Boyd, P. *et al.* Mesoscale iron-enrichment experiments 1993–2005: synthesis and future directions. *Science* **315,** 612–617 (2007).
6. Cassar, N. *et al.* The Southern Ocean biological response to aeolian iron deposition. *Science* **317,** 1067–1070 (2007).
7. Hamme, R. C. *et al.* Volcanic ash fuels anomalous plankton bloom in subarctic northeast Pacific. *Geophys. Res. Lett.* **37,** L19604 (2010).
8. Lampitt, R. S. *et al.* Material supply to the abyssal seafloor in the Northeast Atlantic. *Prog. Oceanogr.* **50,** 27–63 (2001).
9. Abelmann, A., Gersonde, R., Cortese, G., Kuhn, G. & Smetacek, V. Extensive phytoplankton blooms in the Atlantic sector of the glacial Southern Ocean. *Paleoceanography* **21,** PA1013 (2006).
10. Kohfeld, K. E., Le Quéré, C., Harrison, S. P. & Anderson, R. F. Role of marine biology in glacial-interglacial CO_2 cycles. *Science* **308,** 74–78 (2005).
11. The Royal Society. *Geoengineering the Climate: Science, Governance and Uncertainty*. RS policy document 10/09 (The Royal Society, 2009).
12. Chelton, D. B., Schlax, M. G., Samelson, R. M. & de Szoeke, R. A. Global observations of large oceanic eddies. *Geophys. Res. Lett.* **34,** L15606 (2007).
13. d'Ovidio, F., Isern-Fontanet, J., Lopez, C., Hernandez-Garcia, E. & Garcia-Ladona, E. Comparison between Eulerian diagnostics and finite-size Lyapunov exponents computed from altimetry in the Algerian basin. *Deep Sea Res. Part I Oceanogr. Res. Pap.* **56,** 15–31 (2009).
14. Hibbert, A., Leach, H., Strass, V. & Cisewski, B. Mixing in cyclonic eddies in the Antarctic Circumpolar Current. *J. Mar. Res.* **67,** 1–23 (2009).
15. Cisewski, B., Strass, V. H., Losch, M. & Prandke, H. Mixed layer analysis of a mesoscale eddy in the Antarctic Polar Front Zone. *J. Geophys. Res.* **113,** C05017 (2008).
16. Jacquet, S. H. M., Savoye, N., Dehairs, F., Strass, V. H. & Cardinal, D. D. Mesopelagic carbon remineralization during the European Iron Fertilization Experiment. *Glob. Biogeochem. Cycles* **22,** GB1023 (2008).
17. Paytan, A. & McLaughlin, K. The oceanic phosphorus cycle. *Chem. Rev.* **107,** 563–576 (2007).
18. Bishop, J. K. B., Wood, T. J., Davis, R. E. & Sherman, J. T. Robotic observations of enhanced carbon biomass and export at 55° S during SOFeX. *Science* **304,** 417–420 (2004).
19. Jackson, G. A. A model of the formation of marine algal flocs by physical coagulation processes. *Deep-Sea Res.* **37,** 1197–1211 (1990).
20. Riebesell, U. & Wolf-Gladrow, D. A. The relationship between physical aggregation of phytoplankton and particle flux: a numerical model. *Deep-Sea Res. A* **39,** 1085–1102 (1992).
21. de Baar, H. J. W. *et al.* Synthesis of iron fertilization experiments: from the iron age in the age of enlightenment. *J. Geophys. Res.* **110,** C09S16 (2005).
22. Blain, S. *et al.* Effect of natural iron fertilization on carbon sequestration in the Southern Ocean. *Nature* **446,** 1070–1074 (2007).
23. Pollard, R. *et al.* Southern Ocean deep-water carbon export enhanced by natural iron fertilization. *Nature* **457,** 577–580 (2009).
24. Beaulieu, S. E. in *Oceanography and Marine Biology. An Annual Review* (eds Gibson, R. N., Barnes, M. & Atkinson, R. J.) 171–232 (Taylor & Francis, 2002).

Supplementary Information is linked to the online version of the paper at www.nature.com/nature.

Acknowledgements We thank C. Balt, K. Loquay, S. Mkatshwa, H. Prandke, H. Rohr, M. Thomas and I. Vöge for help on board. We are also grateful to U. Struck for POC and PON analyses. The altimeter products were produced by Ssalto/Duacs and distributed by Aviso with support from Cnes. We thank the captain and crew of RV *Polarstern* (cruise ANT XXI/3) for support throughout the cruise.

Author Contributions V.S. and C.K. wrote the manuscript. V.S. directed the experiment and C.K. carried out the budget calculations. V.H.S., P.A., M.M. and D.W.-G. contributed to the preparation of the manuscript. V.H.S., B.C., H.L. and M.L. contributed physical data on mixed-layer depth dynamics, eddy coherence, patch movement and transmissometer data. N.S. provided thorium data. A.W. provided nutrient data. P.A. and J.H. provided phytoplankton and BSi data. F.D. carried out the Lagrangian analysis based on delayed-time altimetry. J.M.A. and G.J.H. provided bacterial data. C.N. and R.B. provided inorganic carbon data. G.M.B., C.K. and M.M.M. provided POC and PON data. P.C. provided the iron data. S.G. and A.T. provided DOM data. I.P. and L.J.H. performed the ^{14}C primary production measurements and provided high-pressure liquid chromatography data. R.R. provided data on photochemical efficiency (F_v/F_m). C.K., M.M.S. and A.T. provided Chl data. U.B., E.S., O.S. and J.S. provided data on the eddy core from a subsequent cruise and satellite Chl images.

Author Information Reprints and permissions information is available at www.nature.com/reprints. The authors declare no competing financial interests. Readers are welcome to comment on the online version of this article at www.nature.com/nature. Correspondence and requests for materials should be addressed to V.S. (victor.smetacek@awi.de) or C.K. (christine.klaas@awi.de).